

http://pubs.acs.org/journal/aelccp

# Nonaqueous Organic Slurry Battery over 4 V

Rajeev K. Gautam, Jack J. McGrath, Xiao Wang, and Jianbing Jimmy Jiang\*



Downloaded via UNIV OF CINCINNATI on September 23, 2024 at 15:38:09 (UTC). See https://pubs.acs.org/sharingguidelines for options on how to legitimately share published articles.

Cite This: ACS Energy Lett. 2024, 9, 4408-4413



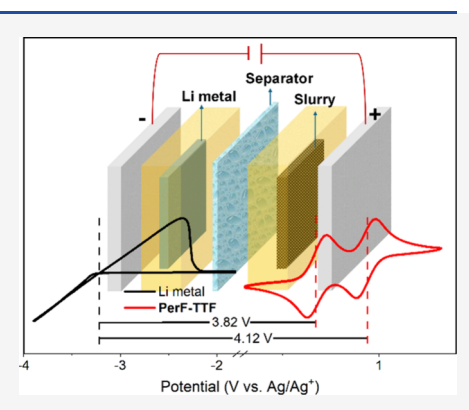
**ACCESS** I

III Metrics & More

Article Recommendations

Supporting Information

ABSTRACT: The development of high-voltage batteries is increasingly desirable because they offer higher energy density than conventional batteries, allowing for greater energy storage over extended periods. Herein, we developed a high-voltage nonaqueous, all-organic slurry battery utilizing molecularly engineered tetrathiafulvalene (TTF) derivatives as redox-active cathode materials. Both perF-TTF and  $CN_4$ -TTF exhibit two reversible one-electron redox activities. The high insolubilities of perF-TTF and CN<sub>4</sub>-TTF in aqueous and nonaqueous electrolyte solutions make them suitable candidates for the development of slurry batteries. The LillperF-TTF (0.5 M) slurry battery exhibited higher performance, showing Coulombic, voltage, and energy efficiencies of 95%, 83%, and 79%, respectively, and capacity retention of 76% over 100 charge/discharge cycles. The LillperF-TTF (0.5 M) slurry battery demonstrated an energy density of ~94 Wh/L and a maximum power density of 251 mW/cm<sup>2</sup>. These findings highlight the potential of slurry batteries for further advancements in battery technology.



rid energy storage is pivotal for advancing sustainable electricity generation, addressing renewable source intermittency, optimizing fossil fuel efficiency through load leveling, and supporting backup power and frequency regulation. 1-3 Redox flow batteries (RFBs), electrochemical systems scaling power and energy density independently, have emerged as promising candidates for grid-scale energy storage.<sup>4,5</sup> RFBs store energy using redox-active molecules in liquid electrolyte solutions, strategically placed in anolyte and catholyte tanks. RFBs are categorized into aqueous (ARFBs) and nonaqueous RFBs (NRFBs) based on the type of electrolyte solutions used. ARFBs have been widely studied for energy storage applications and offer safety and cost advantages. However, they suffer from a narrow electrochemical voltage window (<1.2 V), 8 resulting in a relatively low energy density of 20–50 Wh/L. 5,9 NRFBs face challenges such as solvent flammability, high cost, and low ionic conductivity. 10 Despite these issues, NRFBs stand out with the distinctive advantage of a wider electrochemical window (~5.5 V), 11-15 representing a promising opportunity to incorporate redox-active materials with high redox potential to enhance the energy density of RFBs. 16 However, nonaqueous electrolytes frequently encounter solubility issues, restricting the energy density of active materials in NRFBs.4,17,18

Redox-active materials that are completely insoluble in aqueous and nonaqueous electrolyte solutions cannot be employed in conventional RFB configurations. Nevertheless, employing these materials in the form of a solid slurry, pastelike slurry, or semisolid slurry electrode may be an effective approach for harnessing the potential of such redox-active

materials for energy storage applications. This methodology involves the formation of a slurry of solid electroactive materials mixed with conductive additives (e.g., carbon black) and an electrolyte solution, creating a percolating conductive network. Chiang et al. successfully showcased high-energy density semisolid lithium flow batteries (SSFBs). 19,20 This approach offers the potential advantage of producing batteries with a charge storage density more than ten times higher than conventional RFBs. Consequently, various other research groups have adopted this semisolid slurry electrode approach for different battery chemistries, such as Na-ion, <sup>21</sup> Li–S, <sup>22,23</sup> Zn-MnO<sub>2</sub>, <sup>24</sup> Zn–Ni, <sup>25,26</sup> and many more in organic electrolytes.

In addition, the SSFB approach can also be applied to aqueous electrolyte systems, e.g., slurry batteries based on vanadium and LiFePO<sub>4</sub> chemistries, expanding the scope of its potential applications in energy storage relying on aqueous electrolytes. 34-37 However, the semisolid electrode, characterized by a suspension-type design, unfortunately, introduces a conflict between the energy density of SSFB and the fluidity of its suspension.<sup>32</sup> Increasing the active substance content in the suspension enlarges battery energy density but significantly degrades the flow ability of the semisolid electrode. The

Received: May 31, 2024 Revised: August 5, 2024 Accepted: August 12, 2024 Published: August 16, 2024





conductive network in SSFBs, formed with additives such as carbon black, creates an unstable electronic conductivity known as a percolating network, leading to poor cycle performance under high current density. Furthermore, the flow requirements of the semisolid electrode necessitate more expensive reciprocating pump technologies than the common centrifugal pump used in solution-based flow batteries.

Despite these challenges, ongoing research aims to address the flow of highly viscous semisolid electrodes at a lower cost. <sup>24,26,31</sup> Although this approach has shown promise for solid electroactive inorganic materials, it has rarely been explored for organic materials. Only a few studies have reported insoluble organic materials in slurry batteries with low cell voltage ranging from 1.0 to 1.5 V. <sup>16,38,39</sup> However, due to the low cell voltage and the low volumetric energy density of organic redox-active compounds, the energy density of aqueous slurry batteries remains limited. Hence, organic materials with higher redox potentials are critical for enhancing the performance of these batteries.

In this study, we developed an all-nonaqueous organic slurry battery using molecularly designed highly insoluble tetrathiafulvalene (TTF) based redox-active organic cathodes. The strategy of using electron-withdrawing groups to tune the redox potential of electroactive materials is well-established in organic batteries. Functional groups such as -CF<sub>3</sub>, -NO<sub>2</sub>, -NR<sub>3</sub><sup>+</sup>, -SO<sub>3</sub>H, -COOH, -perF, and -CN increase electron affinity, lowering the highest occupied molecular orbital energy and raising the redox potential. Therefore, TTF was derivatized with perF (perF-TTF) and CN<sub>4</sub> (CN<sub>4</sub>-TTF) substituents, significantly improving its redox potential due to their strong electron-withdrawing effects. These groups pull electron density away from TTF, resulting in higher redox potential and enhanced performance in battery applications. Both perF-TTF and CN<sub>4</sub>-TTF exhibit two reversible oneelectron redox activities at 0.62 and 0.92 V vs Ag/Ag<sup>+</sup> for the first electron and 0.96 and 1.10 V vs Ag/Ag+ for the second electron, respectively. These values are significantly higher than those previously reported for organic materials used in slurry batteries. The Li metal anode was paired with conductive slurries of perF-TTF and CN<sub>4</sub>-TTF in a nonaqueous electrolyte to form LillperF-TTF and LillCN<sub>4</sub>-TTF slurry batteries. The electrochemical kinetics of the slurries were investigated by cyclic voltammetry (CV) and electrochemical impedance spectroscopy (EIS). The cycling performance of the slurry batteries was assessed using prolonged charge/ discharge tests. Slurry batteries with different concentrations of perF-TTF (0.2, 0.5, and 0.75 M) and CN<sub>4</sub>-TTF (0.2 M) were investigated using extended charge/discharge tests.

Preparation and Optimization of Ketjen Black in perF-TTF and CN<sub>4</sub>-TTF Slurries. High charge transfer during charging/discharging of a slurry battery requires a uniform conducting network, often referred to as a percolating network, within the slurry. Ketjen black (KB) is the preferred additive conductive material for such purposes because of its highly porous structure and excellent electrical conductivity. He electro-conductive slurry involves mixing organic redox-active materials, perF-TTF (Figure 1A) or CN<sub>4</sub>-TTF (Figure 1B), with varying amounts of KB. Before introducing the supporting electrolytes, the redox compound and KB were thoroughly mixed using a mortar and pestle for 1 h to ensure an even distribution of the conducting network of KB chains in the composite slurry. Achieving a uniform distribution of slurry

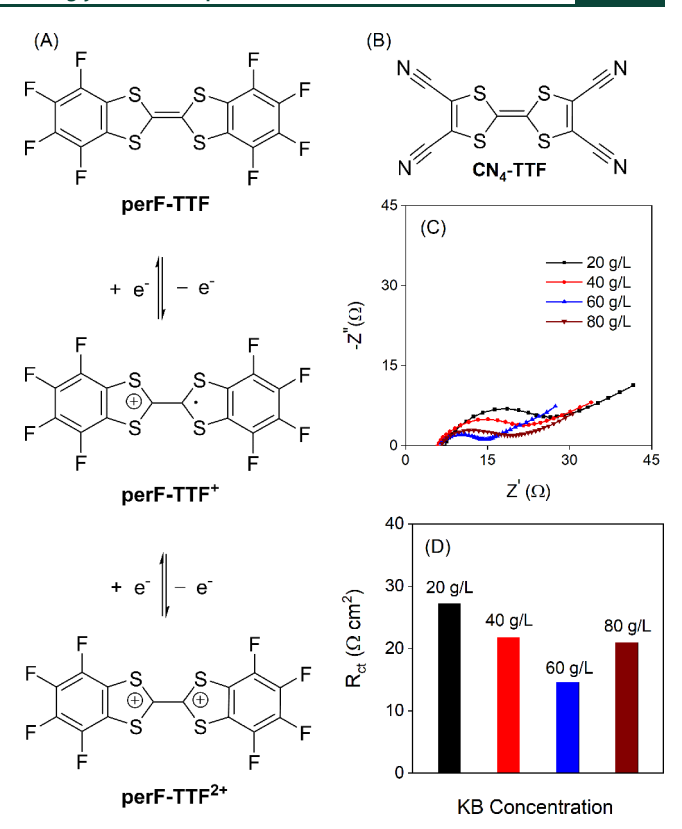


Figure 1. (A) Redox reaction of perF-TTF. (B) Chemical structures of  $CN_4$ -TTF. (C) Electrochemical impedance spectroscopy results for various KB concentrations (20, 40, 60, and 80 g/L). (D) Variation in charge transfer resistance ( $R_{\rm ct}$ ) as a function of KB concentration in the perF-TTF (0.5 M) slurry.

constituents is crucial for promoting efficient redox reactions and optimizing the capacity utilization of the redox-active materials. To determine the optimal KB loading for a given perF-TTF or CN<sub>4</sub>-TTF concentration, various KB concentrations (10, 15, 20, 25, 40, 60, and 80 g/L) were prepared in a solution of dimethyl carbonate (DMC)/lithium hexafluor-ophosphate (LiPF<sub>6</sub>) (1 M) and tetraethylene glycol dimethyl ether (TEGDME) (5% by volume). TEGDME was used to enhance the homogeneity of KB within the slurry. Slurries of perF-TTF or CN<sub>4</sub>-TTF with different KB concentrations were analyzed using EIS.

The solution resistance (R<sub>s</sub>) remains consistent across all KB concentrations, while the charge transfer resistance (R<sub>ct</sub>) varies noticeably. A higher R<sub>ct</sub> implies poor electrocatalytic behavior or high charge transport losses in the developed slurry. At a low KB loading of 20 g/L, the slurry exhibits a substantial R<sub>ct</sub> value (26  $\Omega$  cm<sup>2</sup>) due to a poorly conducting network formed by the limited KB particle loading (Figure 1C and 1D). However, as the KB concentrations increase from 20 to 60 g/ L,  $R_{ct}$  decreases from 27 to 14  $\Omega$  cm<sup>2</sup>. This reduction is attributed to the higher conducting network in the slurry, which is facilitated by the well-connected KB and perF-TTF molecules. A KB concentration of 60 g/L yielded the lowest R<sub>ct</sub> value, ensuring an optimal distribution of conducting KB chains within the perF-TTF slurry (Figure S1). The surface morphology (Figure S2A) and elemental distribution of the slurry at 60 g/L (Figure S2B-S2F) suggest a uniform distribution of the slurry constituents. However, a further increase in KB loading (80 g/L) resulted in an elevated R<sub>ct</sub> indicating poor charge transfer in the slurry, potentially owing

ACS Energy Letters http://pubs.acs.org/journal/aelccp Letter

to KB particle aggregation. Hence, a KB loading of 60 g/L was selected for subsequent studies. Similarly, the  $CN_4$ -TTF slurry exhibited an optimal KB concentration of 20 g/L (Figure S3A and S3B).

**Electrochemical Characterization.** The electrochemical properties of the **perF-TTF** and  $\text{CN}_4\text{-TTF}$  slurries were characterized using CV in a DMC/LiPF<sub>6</sub> (0.1 M) electrolyte at a scan rate of 50 mV/s (Figure 2A). The **perF-TTF** and  $\text{CN}_4\text{-}$ 

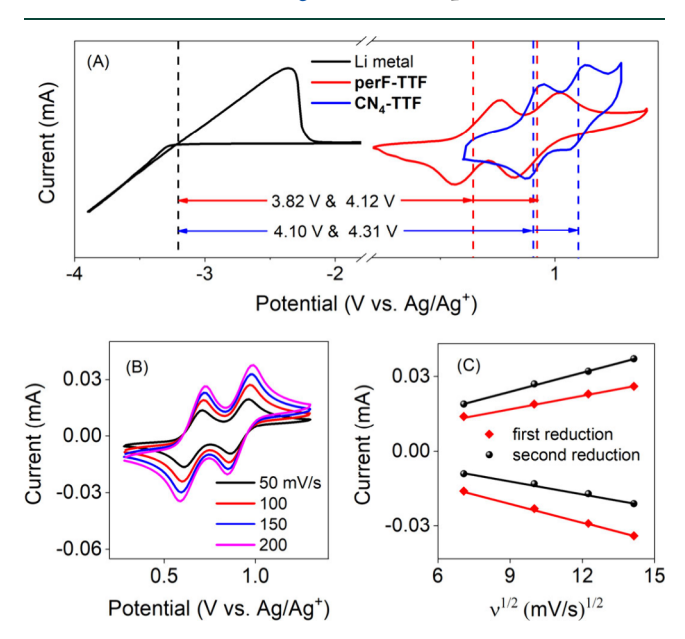


Figure 2. (A) Cyclic voltammograms of Li metal, perF-TTF slurry, and CN<sub>4</sub>-TTF slurry in DMC/LiPF<sub>6</sub> (0.1 M) at a scan rate of 50 mV/s. (B) Cyclic voltammograms of perF-TTF slurry at varying scan rates of 50–200 mV/s. (D) Current vs square root curve of scan rate curves of the perF-TTF slurry for first and second reduction.

TTF slurries exhibit two reversible one-electron redox processes with well-defined redox potential peaks at 0.62 and 0.96 V (vs Ag/Ag<sup>+</sup>), respectively, for the first reduction and 0.92 and 1.10 V (vs Ag/Ag<sup>+</sup>) for the second reduction (Figure 2A). When paired with Li metal, perF-TTF and CN<sub>4</sub>-TTF can provide cell voltages of 3.82 and 4.10 V, respectively, for the first electron and 4.12 and 4.31 V for the second electron. These voltages are significantly higher than other organic redox materials used in slurry batteries.  $^{16,38}$ 

Furthermore, the electrokinetic behavior of the **perF-TTF** slurry was evaluated by varying the scan rates from 50 to 200 mV/s (Figure 2B). Nernstian peak separations of 78 (first reduction) and 79 mV (second reduction) indicated one-electron redox processes. The linear relationship between the oxidation and reduction peak currents ( $i_p$ ) for the first and second reductions suggested diffusion-controlled redox reactions (Figure 2C). The  $i_{pc}/i_{pa}$  ratio approached 1 for both reductions (Figure S4), indicating excellent electrochemical reversibility.

Charge/Discharge Performance of perF-TTF and CN<sub>4</sub>-TTF Slurry Batteries. The charge/discharge test is crucial for evaluating cathode and anode materials in batteries through the analysis of voltage profiles and discharge characteristics, offering key insights into their electrochemical behavior.

To assess the compatibility of perF-TTF in the slurry and its interaction with the Li metal anode, long-term charge/

discharge cycling of a low-concentration (0.2 M) slurry battery (Figure S5) was conducted. The LillperF-TTF (0.2 M) slurry battery was tested over 100 charge/discharge cycles (9 d) at a charge/discharge current density of 2 mA/cm², which yielded a capacity retention of 88.66% (98.74% per day, 99.88 per cycle) and a theoretical capacity utilization of 93% (Figure 3A). In addition, the battery exhibited a CE, VE, and EE of

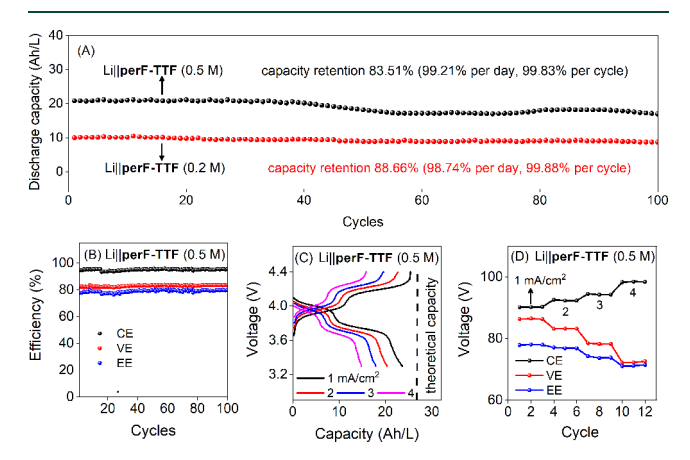


Figure 3. (A) Capacity retention of LillperF-TTF (0.2 and 0.5 M) slurry batteries. (B) Coulombic efficiency (CE), voltage efficiency (VE), and energy efficiency (EE) of the LillperF-TTF (0.5 M) slurry battery. (C) Charge/discharge curves of the LillperF-TTF (0.5 M) battery at different current densities. (D) Variation in the CE, VE, and EE of LillperF-TTF (0.5 M) at different current densities (three cycles each).

98.23%, 86.32%, and 84.79%, respectively (Figure S6). Postcycle EIS analysis (Figure S7) showed a slight increase in both  $R_s$  and  $R_{ct}$ , which could be attributed to solvent loss under prolonged battery cycling.

The charge/discharge performance of the LillCN<sub>4</sub>-TTF (0.2 M) slurry battery was also evaluated. Unlike the LillperF-TTF (0.2 M) slurry battery, the LillCN<sub>4</sub>-TTF (0.2 M) slurry battery exhibited faster capacity fading, with an average CE of 83% (for three cycles, Figure S8A). Postcycle EIS analysis (Figure S8B) revealed a notable increase in  $R_{\rm ct}$  compared with that of the precycled battery. The sharp increase in  $R_{\rm ct}$  can be attributed to the substantial phase separation of the slurry constituents during charging/discharging. The higher  $R_{\rm ct}$  value, suggesting poor charge-transport kinetics, resulted in faster capacity fading. This phase separation could be the major reason for the rapid capacity fading of the LillCN<sub>4</sub>-TTF slurry battery.

To observe the impact of the electrolyte system, LillCN<sub>4</sub>-TTF (0.2 M) slurry batteries using the DMC:PC (80:20, v:v)/LiPF<sub>6</sub> and DMC:EMC (80:20, v:v)/LiPF<sub>6</sub> electrolyte systems were developed. Both slurry batteries were tested for their charge/discharge performance, as shown in Figures S9A and S10A. However, both batteries displayed charge/discharge behavior similar to that of the LillCN<sub>4</sub>-TTF slurry battery using DMC/LiPF<sub>6</sub> (1 M) (Figure S8A), with poor capacity retention. Both postcycling batteries displayed higher R<sub>ct</sub> values (Figures S9B and S10B), suggesting substantial phase separation of the slurry constituents, consequently resulting in poor charge-transport kinetics and faster capacity fading. Because of the poor performance of CN<sub>4</sub>-TTF, further studies on this compound were discontinued.

ACS Energy Letters http://pubs.acs.org/journal/aelccp Letter

Following the successful demonstration of the LillperF-TTF (0.2 M) slurry battery, to enhance the energy density, we evaluated a higher-concentration slurry battery with a perF-TTF concentration of 0.5 M. The long-term cycling performance of the LillperF-TTF (0.5 M) battery was assessed over 100 charge/discharge cycles (21 days) at a current density of 2 mA/cm<sup>2</sup>. The battery displayed a capacity retention of 83.51% (99.21% per day, 99.83% per cycle) and a capacity utilization of  $\sim$ 78% (Figure 3A). Furthermore, the LillperF-TTF (0.5 M) slurry battery displayed a CE, VE, and EE of 95.15%, 83.10%, and 79.06%, respectively (Figure 3B). Postcycling EIS analysis (Figure S11) revealed an increase in R<sub>s</sub>, which may be attributed to slurry dryness during extended battery operation. The reduction in the solvent content of the slurry significantly affected the capacity retention of the battery. As the battery becomes dry, its capacity deteriorates more rapidly owing to the phase separation of the slurry under prolonged operational conditions. The rate performance of the LillperF-TTF (0.5 M) battery was studied at 1, 2, 3, and 4 mA/cm<sup>2</sup> with three continuous charge/discharge cycles at each current density (Figure 3C). As the current density increased from 1 to 4 mA/ cm<sup>2</sup>, the capacity utilization decreased from 88.2% to 55.2%. The charge/discharge overpotential increased with increasing current density owing to mass transport limitations, which resulted in decreased capacity utilization. As shown in Figure 3D, the CE of the battery increased with increasing current density, which is likely due to the improved electrochemical reversibility and reduced side reactions, leading to more efficient charging and discharging. However, the VE and EE decreased from 86.35% and 77.89% to 72.65% and 75.51%, respectively, as the current density increased from 1 to 4 mA/ cm<sup>2</sup>. As the current density increased, the battery experienced greater polarization effects, leading to increased resistance and energy losses during the charge and discharge processes. The elevated overpotential resulted in a reduced VE, indicating that a larger portion of the input energy is lost as overpotential losses than is efficiently utilized for the desired electrochemical reactions.

To further enhance the energy density and showcase the adaptability of perF-TTF, we investigated the LillperF-TTF slurry battery with a perF-TTF concentration of 0.75 M. The battery was cycled for 100 charge/discharge cycles (8 d), revealing a modest capacity retention of 51.53% (93.94% per day and 99.51% per cycle). This performance was accompanied by a CE, VE, and EE of 95.15%, 85.54%, and 81.39%, respectively, as shown in Figure S12. The poor capacity retention is attributed to the inadequate wettability of perF-TTF molecules at higher concentrations. This leads to an unstable battery capacity with eventual phase separation owing to the hindered wetting of active particles, resulting in faster capacity fading. Experimental evidence supporting this assertion was derived from EIS measurements (Figure S13) of the postcycled battery, where an increase in cell resistance was evident compared to the LillperF-TTF (0.5 M) slurry battery.

The power density of the LillperF-TTF (0.5 M) slurry battery was investigated for state of the charge (SOC) values ranging from 100% to 25%. The slurry battery exhibited a maximum power density of 251 mW/cm², as shown in Figure 4A. Moreover, the investigation of area-specific resistance revealed a decreasing trend with increasing SOC values (Figure 4B). Both cell- and membrane-specific resistances exhibited this behavior. Notably, the resistance across the separator was

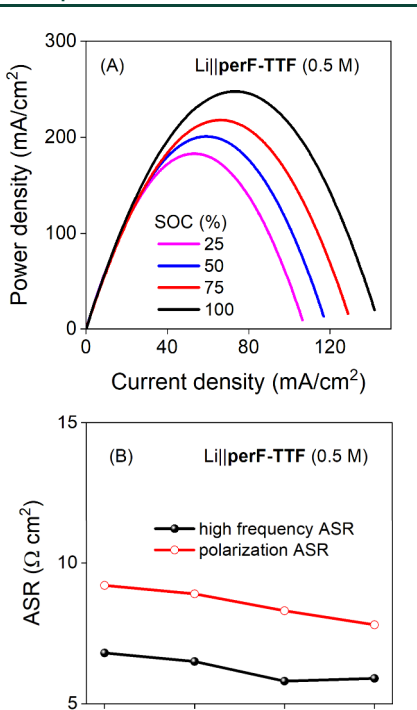


Figure 4. (A) Power density curve of the LillperF-TTF (0.5 M) slurry battery at 100%, 75%, 50%, and 25% state of charge (SOC). (B) Variation of high-frequency area-specific resistance (ASR) and polarization ASR of LillperF-TTF (0.5 M) slurry battery at different SOC values.

50

SOC (%)

75

100

60% that of the entire cell, further contributing to a comprehensive understanding of the electrochemical performance of the system. Furthermore, owing to the elevated redox potential of, the slurry battery with a perF-TTF concentration of 0.5 M achieved an energy density of 94 Wh/L. The LillperF-TTF (0.5 M) slurry battery exhibited a high average discharge voltage and energy density compared to previously reported organic slurry batteries, 16,38 while demonstrating comparable performance to slurry batteries based on inorganic insoluble materials (Figure 5 and Table S2). 20–25,28,31,42

In summary, a high-voltage nonaqueous all-organic slurry battery based on highly insoluble TTF derivatives (perF-TTF and CN<sub>4</sub>-TTF) with a cell voltage of over 4 V was successfully demonstrated for the first time. The molecular design of the TTF compound involved attaching PerF and CN<sub>4</sub> chains to the TTF framework, which significantly improved the redox

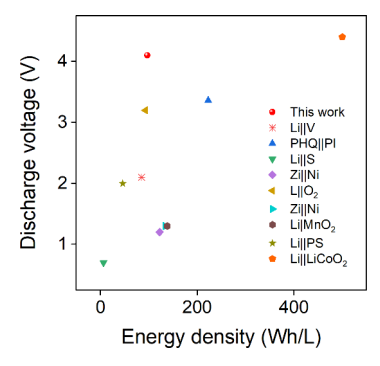


Figure 5. Comparison of average discharge voltages and energy densities of previously reported semisolid batteries.

potential significantly of TTF. Both perF-TTF, and CN<sub>4</sub>-TTF exhibited two reversible one-electron redox activities. Conducting organic slurries of perF-TTF and CN4-TTF were prepared using KB. Organic cathodic slurries of perF-TTF and CN<sub>4</sub>-TTF were paired with a Li metal anode to create a highvoltage nonaqueous slurry battery. The performance of slurry batteries with different concentrations (0.2, 0.5, and 0.75 M) of redox-active materials were studied. The LillperF-TTF (0.5 M) slurry battery displayed the highest performance, with a CE, VE, EE of 95%, 83%, and 79%, and capacity retention of 89% over 100 charge/discharge cycles. Moreover, the organic slurry battery demonstrated an energy density of 94 Wh/L and a maximum power density of 251 mW/cm<sup>2</sup>. The performance of the LillperF-TTF slurry batteries was considerably higher than that of previously reported organic slurry batteries and was comparable to that of slurry batteries based on inorganic insoluble materials. These results highlight the significant potential of slurry batteries for further advancements in battery technology.

#### ASSOCIATED CONTENT

## Supporting Information

The Supporting Information is available free of charge at https://pubs.acs.org/doi/10.1021/acsenergylett.4c01470.

Experimental methods; additional figures, including SEM images, EDS images, and EIS measurements; Coulombic and energy efficiencies; literature comparison of various semisolid slurry batteries (PDF)

## AUTHOR INFORMATION

#### **Corresponding Author**

Jianbing Jimmy Jiang — Department of Chemistry, University of Cincinnati, Cincinnati, Ohio 45221-0172, United States; orcid.org/0000-0002-7466-522X;

Email: jianbing.jiang@uc.edu; www.jianbingjiang.com

### **Authors**

Rajeev K. Gautam — Department of Chemistry, University of Cincinnati, Cincinnati, Ohio 45221-0172, United States Jack J. McGrath — Department of Chemistry, University of Cincinnati, Cincinnati, Ohio 45221-0172, United States Xiao Wang — Department of Chemistry, University of Cincinnati, Cincinnati, Ohio 45221-0172, United States

Complete contact information is available at: https://pubs.acs.org/10.1021/acsenergylett.4c01470

#### Notes

The authors declare no competing financial interest.

#### ACKNOWLEDGMENTS

This study was supported by the National Science Foundation (Grant No. CBET-2112798).

# **■** REFERENCES

- (1) Noack, J.; Roznyatovskaya, N.; Herr, T.; Fischer, P. The Chemistry of Redox-Flow Batteries. *Angew. Chem., Int. Ed.* **2015**, 54 (34), 9776–9809.
- (2) Yin, J.; Molini, A.; Porporato, A. Impacts of Solar Intermittency on Future Photovoltaic Reliability. *Nat. Commun.* **2020**, *11* (1), 4781.
- (3) Obama, B. The Irreversible Momentum of Clean Energy. *Science* **2017**, 355 (6321), 126–129.

- (4) Wang, W.; Luo, Q.; Li, B.; Wei, X.; Li, L.; Yang, Z. Recent Progress in Redox Flow Battery Research and Development. *Adv. Funct. Mater.* **2013**, 23 (8), 970.
- (5) Sánchez-Díez, E.; Ventosa, E.; Guarnieri, M.; Trovò, A.; Flox, C.; Marcilla, R.; Soavi, F.; Mazur, P.; Aranzabe, E.; Ferret, R. Redox Flow Batteries: Status and Perspective Towards Sustainable Stationary Energy Storage. *J. Power Sources* **2021**, *481*, 228804.
- (6) Soloveichik, G. L. Flow Batteries: Current Status and Trends. Chem. Rev. 2015, 115 (20), 11533-11558.
- (7) Wang, X.; Gautam, R. K.; Jiang, J. J. Strategies for Improving Solubility of Redox-Active Organic Species in Aqueous Redox Flow Batteries: A Review. *Batteries Supercaps* **2022**, 5 (11), No. e202200298.
- (8) Xu, K.; Wang, C. Batteries: Widening Voltage Windows. *Nat. Energy* **2016**, *1* (10), 16161.
- (9) Huang, Y.; Gu, S.; Yan, Y.; Li, S. F. Y. Nonaqueous Redox-Flow Batteries: Features, Challenges, and Prospects. *Curr. Opin. Chem. Eng.* **2015**, *8*, 105–113.
- (10) Rhodes, Z.; Cabrera-Pardo, J. R.; Li, M.; Minteer, S. D. Electrochemical Advances in Non-Aqueous Redox Flow Batteries. *Isr. J. Chem.* **2021**, *61* (1–2), 101–112.
- (11) Gautam, R. K.; Wang, X.; Lashgari, A.; Sinha, S.; McGrath, J.; Siwakoti, R.; Jiang, J. Development of High-Voltage and High-Energy Membrane-Free Nonaqueous Lithium-Based Organic Redox Flow Batteries. *Nat. Commun.* **2023**, *14* (1), 4753.
- (12) Gautam, R. K.; Wang, X.; Sinha, S.; Jiang, J. Triphasic Electrolytes for Membrane-Free High-Voltage Redox Flow Battery. ACS Energy Lett. 2024, 9 (1), 218–225.
- (13) Jia, C.; Pan, F.; Zhu, Y. G.; Huang, Q.; Lu, L.; Wang, Q. High-Energy-Density Nonaqueous All Redox Flow Lithium Battery Enabled with a Polymeric Membrane. *Sci. Adv.* **2015**, *1* (10), No. e1500886.
- (14) Wei, X.; Duan, W.; Huang, J.; Zhang, L.; Li, B.; Reed, D.; Xu, W.; Sprenkle, V.; Wang, W. A High-Current, Stable Nonaqueous Organic Redox Flow Battery. ACS Energy Lett. 2016, 1 (4), 705–711.
- (15) Yu, X.; Manthiram, A. Accessing a High-Voltage Nonaqueous Hybrid Flow Battery with a Sodium-Methylphenothiazine Chemistry and a Sodium-Ion Solid Electrolyte. *Energy Storage* **2022**, *4* (1), No. e281.
- (16) Wang, X.; Lashgari, A.; Siwakoti, R.; Gautam, R. K.; McGrath, J. J.; Sarkar, P.; Naber, G.; Chai, J.; Jiang, J. Tetrathiafulvalene (TTF) Derivatives as Catholytes for Dual-Type Redox Flow Batteries: Molecular Engineering Enables High Energy Density and Cyclability. *J. Mater. Chem. A* **2023**, *11* (35), 19056–19065.
- (17) Li, M.; Case, J.; Minteer, S. D. Bipolar Redox-Active Molecules in Non-Aqueous Organic Redox Flow Batteries: Status and Challenges. *ChemElectroChem.* **2021**, *8* (7), 1215–1232.
- (18) Wang, X.; Chai, J.; Jiang, J. Redox Flow Batteries Based on Insoluble Redox-Active Materials. A Review. *Nano Mater. Sci.* **2021**, 3 (1), 17–24.
- (19) Duduta, M.; Ho, B.; Wood, V. C.; Limthongkul, P.; Brunini, V. E.; Carter, W. C.; Chiang, Y. M. Semi-solid Lithium Rechargeable Flow Battery. *Adv. Energy Mater.* **2011**, *1* (4), 511–516.
- (20) Wei, T. S.; Fan, F. Y.; Helal, A.; Smith, K. C.; McKinley, G. H.; Chiang, Y. M.; Lewis, J. A. Biphasic Electrode Suspensions for Li-Ion Semi-Solid Flow Cells with High Energy Density, Fast Charge Transport, and Low-Dissipation Flow. *Adv. Energy Mater.* **2015**, 5 (15), 1500535.
- (21) Ventosa, E.; Buchholz, D.; Klink, S.; Flox, C.; Chagas, L. G.; Vaalma, C.; Schuhmann, W.; Passerini, S.; Morante, J. R. Nonaqueous Semi-solid Flow Battery Based on Na-ion Chemistry. P2-type Na<sub>x</sub>Ni<sub>0.22</sub>Co<sub>0.11</sub>Mn<sub>0.66</sub>O<sub>2</sub>-NaTi<sub>2</sub>(PO<sub>4</sub>)<sub>3</sub>. *Chem. Commun.* **2015**, *51* (34), 7298–7301.
- (22) Wang, C.; Lai, Q.; Xu, P.; Li, X.; Zhang, H. A Non-Aqueous Li/ Organosulfur Semi-Solid Flow Battery. *Chin. Chem. Lett.* **2018**, 29 (5), 716–718
- (23) Chen, H.; Zou, Q.; Liang, Z.; Liu, H.; Li, Q.; Lu, Y. C. Sulphur-Impregnated Flow Cathode to Enable High-Energy-Density Lithium Flow Batteries. *Nat. Commun.* **2015**, *6*, 5877.

- (24) Narayanan, T. M.; Zhu, Y. G.; Gençer, E.; McKinley, G.; Shao-Horn, Y. Low-Cost Manganese Dioxide Semi-Solid Electrode For Flow Batteries. *Joule* **2021**, *5* (11), 2934–2954.
- (25) Zhu, Y. G.; Narayanan, T. M.; Tulodziecki, M.; Sanchez-Casalongue, H.; Horn, Q. C.; Meda, L.; Yu, Y.; Sun, J.; Regier, T.; McKinley, G. H.; Shao-Horn, Y. High-Energy and High-Power Zn-Ni Flow Batteries with Semi-Solid Electrodes. *Sustainable Energy Fuels* **2020**, *4* (8), 4076–4085.
- (26) Liu, Y.; Hu, Q.; Zhong, J.; Wang, Z.; Guo, H.; Yan, G.; Li, X.; Peng, W.; Wang, J. A Renewable Sedimentary Slurry Battery: Preliminary Study in Zinc Electrodes. *iScience* **2020**, 23 (12), 101821.
- (27) Chen, H.; Lu, Y. C. A High-Energy-Density Multiple Redox Semi-Solid-Liquid Flow Battery. *Adv. Energy Mater.* **2016**, 6 (8), 1502183.
- (28) Cheng, S.; Hu, Y.; Jiang, L.; Dang, H.; Ding, Y.; Duan, Q.; Xiao, H.; Sun, J.; Wang, Q. A LiFePO<sub>4</sub> Based Semi-Solid Lithium Slurry Battery for Energy Storage and a Preliminary Assessment of its Fire Safety. *Fire Technol.* **2023**, *59* (3), 1181–1197.
- (29) Chen, M.; Liu, L.; Zhang, P.; Chen, H. A Low-Cost and High-Loading Viologen-Based Organic Electrode for Rechargeable Lithium Batteries. *RSC Adv.* **2021**, *11* (39), 24429–24435.
- (30) Akuzum, B.; Singh, P.; Eichfeld, D. A.; Agartan, L.; Uzun, S.; Gogotsi, Y.; Kumbur, E. C. Percolation Characteristics of Conductive Additives for Capacitive Flowable (Semi-Solid) Electrodes. *ACS Appl. Mater. Interfaces* **2020**, *12* (5), 5866–5875.
- (31) Fan, F. Y.; Woodford, W. H.; Li, Z.; Baram, N.; Smith, K. C.; Helal, A.; McKinley, G. H.; Carter, W. C.; Chiang, Y. M. Polysulfide Flow Batteries Enabled by Percolating Nanoscale Conductor Networks. *Nano Lett.* **2014**, *14* (4), 2210–2218.
- (32) Ventosa, E. Semi-Solid Flow Battery and Redox-Mediated Flow Battery: Two Strategies to Implement the use of Solid Electroactive Materials in High-Energy Redox-Flow Batteries. *Curr. Opin. Chem. Eng.* **2022**, *37*, 100834.
- (33) Soavi, F.; Brilloni, A.; De Giorgio, F.; Poli, F. Semi-Solid Lithium/Oxygen Flow Battery: An Emerging, High-Energy Technology. *Curr. Opin. Chem. Eng.* **2022**, *37*, 100835.
- (34) Yang, Z.; Zhang, Q.; Li, W.; Xie, C.; Wu, T.; Hu, C.; Tang, Y.; Wang, H. A Semi-Solid Zinc Powder-based Slurry Anode for Advanced Aqueous Zinc-ion Batteries. *Angew. Chem., Int. Ed.* **2023**, 62 (3), No. e202215306.
- (35) Aguilo-Aguayo, N.; Hubmann, D.; Khan, F. U.; Arzbacher, S.; Bechtold, T. Water-based Slurries for High-Energy LiFePO<sub>4</sub> Batteries using Embroidered Current Collectors. Sci. Rep. 2020, 10 (1), 5565.
- (36) Li, Z.; Smith, K. C.; Dong, Y.; Baram, N.; Fan, F. Y.; Xie, J.; Limthongkul, P.; Carter, W. C.; Chiang, Y. M. Aqueous Semi-Solid Flow Cell: Demonstration and Analysis. *Phys. Chem. Chem. Phys.* **2013**, *15* (38), 15833–15839.
- (37) Lohaus, J.; Rall, D.; Kruse, M.; Steinberger, V.; Wessling, M. On Charge Percolation in Slurry Electrodes used in Vanadium Redox Flow Batteries. *Electrochem. Commun.* **2019**, *101*, 104–108.
- (38) Yan, W.; Wang, C.; Tian, J.; Zhu, G.; Ma, L.; Wang, Y.; Chen, R.; Hu, Y.; Wang, L.; Chen, T.; Ma, J.; Jin, Z. All-Polymer Particulate Slurry Batteries. *Nat. Commun.* **2019**, *10* (1), 2513.
- (39) Wang, X.; Chai, J.; Zhang, S.; Chen, B.; Chaturvedi, A.; Cui, G.; Jiang, J. Insights Into Indigo K<sup>+</sup> Association in a Half-Slurry Flow Battery. *ACS Energy Lett.* **2022**, *7* (3), 1178–1186.
- (40) Fransson, L.; Eriksson, T.; Edström, K.; Gustafsson, T.; Thomas, J. O. Influence of Carbon Black and Binder on Li-Ion Batteries. *J. Power Sources* **2001**, *101* (1), 1–9.
- (41) Dominko, R.; Gaberšček, M.; Drofenik, J.; Bele, M.; Jamnik, J. Influence of Carbon Black Distribution on Performance of Oxide Cathodes for Li-Ion Batteries. *Electrochim. Acta* **2003**, *48* (24), 3709–3716.
- (42) Perez-Antolin, D.; Schuhmann, W.; Palma, J.; Ventosa, E. Semi-Flowable Zn Semi-Solid Electrodes as Renewable Energy Carrier for Refillable Zn—Air Batteries. *J. Power Sources* **2022**, *536*, 231480.